Instantaneous crankshaft torsional deformation during turbocharged diesel engine operation

E.G. Giakoumis*, I.A. Dodoulas and C.D. Rakopoulos

Thermal Engineering Department,
School of Mechanical Engineering,
National Technical University of Athens,
9 Heroon Polytechniou St.,
Zografou Campus, 15780, Athens, Greece
E-mail: vgiakms@central.ntua.gr
E-mail: i.dodoulas09@imperial.ac.uk
E-mail: cdrakops@central.ntua.gr
*Corresponding author

Abstract: An experimentally validated diesel engine code is used to study the crankshaft torsional deformations originating in the difference between instantaneous engine and load torques. The analysis aims in studying the phenomena under critical conditions, namely operation when one cylinder malfunctions ('open valves' or motoring situation) as well as during transient conditions. A detailed crankshaft torsional model is formulated; this takes into account cylinder gas, inertia, friction, load and stiffness and damping torques. Details are provided concerning the underlying mechanism of the crankshaft torsional deformations, which can assume significant values depending on the specific configuration, being important for safe engine operation.

Biographical notes: Evangelos G. Giakoumis received Dipl.Ing. and Dr.Ing. from the School of Mechanical Engineering of the National Technical University of Athens (NTUA), Greece. He has worked for six years as Area Manager at the After-Sales Department of the Peugeot Automobiles Distributor in Greece, and he is now Assistant Professor at the Thermal Engineering Department of the School of Mechanical Engineering of the NTUA. His research interests include diesel engine experimental and simulation analysis under transient conditions, second-law analysis of internal combustion engines and use of alternative fuels.

Ilias A. Dodoulas received Dipl.Ing. from the School of Mechanical Engineering of the NTUA, Greece. He is currently working on his PhD thesis at Imperial College of Science, Technology and Medicine, University of London, UK.

Constantine D. Rakopoulos is Full Professor of Internal Combustion Engines and Director of the I.C. Engines Laboratory at the School of Mechanical Engineering of the NTUA, Greece. He graduated (Dipl.Ing.) from the NTUA and obtained his MSc, DIC and PhD from Imperial College of Science, Technology and Medicine, University of London, UK. He has been responsible for the development of engines research at the School of Mechanical Engineering of the NTUA for the last 30 years, with over 180 refereed papers in international journals and conferences.

1   Introduction

The turbocharged diesel engine is nowadays the most preferred prime mover in medium and medium-large units' applications (trucks, land traction, ship propulsion, electrical generation). Moreover, it continuously increases its share in the highly competitive automotive market, owing to its reliability that is combined with excellent fuel efficiency. Particularly, its transient operation is of paramount importance in the everyday operating conditions of engines, being often linked with off-design (e.g., turbocharger lag) and, consequently, non-optimum performance and increased exhaust emissions.

During the last decades, mathematical simulation and experimental investigation have paved the way for an in-depth study of diesel engine processes under both steady-state and transient conditions (e.g., Benson and Whitehouse, 1979; Watson and Janota, 1982; Heywood, 1988; Watson, 1981; Rakopoulos and Giakoumis, 2006a, 2009; Black et al., 2007). Particularly, the mathematical tools have become very popular in recent years owing to the continuously increasing improvement in computational power. However, the majority of research has focused so far on thermodynamics, as this directly affects heat release predictions and consequently performance and pollutants emissions. On the other hand, issues concerning the engine dynamics, e.g., connecting rod complex movement, kinematics of the slider–crank mechanism, crankshaft deformations, torsional vibrations, etc., are often disregarded or over-simplified, possibly for the sake of speeding up programme execution time (Rakopoulos and Giakoumis, 2006b).

An important aspect of internal combustion engine operation is that instantaneous engine torque fluctuates significantly during an engine cycle, even under steady-state conditions. The main mechanism behind this is the cyclic nature of gas pressures (4π angular period for a four-stroke engine) and inertia reciprocating forces (2π angular period) (Taylor, 1985). This fluctuation may be of considerable magnitude, particularly during turbocharged diesel engine operation, where the cylinder pressures assume very high values. On the other hand, resistance (load) torque remains practically constant during a cycle (particularly so for industrial or heavy-duty engines as the one under study) owing to the usually adequate non-uniformity of rotation; the latter being, mainly, determined by the flywheel mass moment of inertia and cylinder number and disposition. As a result, a significant fluctuation occurs in the instantaneous net (engine minus load) torque that eventually leads to cyclic speed irregularities, twists between individual cranks of a multi-cylinder engine and, finally, torsional (angular) deformation of the whole elastic crankshaft. Particularly in modern automotive engines, the above-mentioned phenomenon is intensified by the flexibility of lightweight crankshafts that may even lead to 'engine roughness'.

The instantaneous values of crankshaft torsional deformation should be maintained overall low, to avoid excessive stress of the crankshaft and its bearings so that safe engine operation is ensured. To be able to study and quantify this deformation, detailed crankshaft angular momentum equilibrium needs first to be formulated. Apart from the well-known gas, inertia and load terms, this equilibrium must take into account the *instantaneous* values of all other torque contributors, including stiffness, damping and all engine mechanical losses (Piston Rings Assembly (PRA), valve train, bearing, auxiliaries).

Past research on steady-state engine dynamics can prove useful in formulating the crankshaft torsional behaviour model (Rizzoni and Wang, 1985; Haddad, 1995; Taraza et al., 1998; Zweiri et al., 1999; Rahnejat, 2000; Chen and Chen, 1993). However, in all the previous works, the main object of research was either the estimation of indicated torque using, for example, sliding mode observers (Rizzoni and Wang, 1985), or the reconstruction of cylinder pressures from crankshaft angular velocity measurements (Taraza et al., 1998), e.g., for diagnosis purposes (Chen and Chen, 1993); application of finite element methods as a tool for crankshaft analysis has also been a common practice (Murin, 2005). On the other hand, classic torsional vibration handbooks deal with the subject on a cycle rather than degree Crank Angle (ºCA) basis, for the special, but very important, case where the engine operates at resonance with some harmonic order of the exciting engine forces (e.g., Haug, 1952; Ker Wilson, 1959–1969). As regards the very demanding transient diesel engine operation, no effort has been made so far to address torsional deformation effects either as regards the power transmission shaft between engine flywheel and load or between the individual cylinder cranks.

The current work aims at studying the crankshaft angular momentum equilibrium on a detailed dynamic basis, assuming the crankshaft as a flexible, elastic body that may deform during engine operation. Unlike previous research, this crankshaft modelling assumes all possible deformations between engine pulley, cylinder cranks, flywheel and load (and not just the one in the power transmission shaft between the engine and the resistance). Moreover, in our approach, the dynamic model is coupled to a thermodynamic model of the engine processes under both steady-state and transient conditions (Rakopoulos et al., 2004; Rakopoulos and Giakoumis, 2006b). By so doing, it is believed that useful information can be drawn regarding the underlying mechanisms, since the dynamic and the thermodynamic processes are studied in conjunction. Special care is paid to the formulation of the crankshaft torque balance by taking into account, among other things, the instantaneous engine friction torque, using a recently developed detailed friction model, as well as the instantaneous gas torque contribution separately from each cylinder, when studying the transient operation of a multi-cylinder engine.

2 Simulation analysis

2.1 General process description

The present analysis does not, at the moment, include predictions of exhaust gas emissions and, on the other hand, deals with transient operation calculations on a ºCA basis. Therefore, a single-zone model following the filling and emptying approach is used for the evaluation of the thermodynamic processes. This approach is believed to be the best compromise between accuracy and limited PC programme execution time

(Rakopoulos and Giakoumis, 2006b). The species considered are O_2, N_2, CO_2, H_2O and CO; the latter is taken into account, using the corresponding chemical equilibrium scheme, only when the mixture is rich and for gas temperatures exceeding 1400 K, as for example during the early cycles of a transient event, where the turbocharger lag is prominent (Rakopoulos and Giakoumis, 2009).

For heat release rate predictions, the fundamental model proposed by Whitehouse and Way (1969–1970) is used. Especially during transients, the constant K in the (dominant) preparation rate equation of the model is correlated with the Sauter Mean Diameter (SMD) of the fuel droplets, through a formula of the type $K \propto (1/SMD)^{2.5}$ (Benson and Whitehouse, 1979). The improved model of Annand (Annand and Ma, 1970–1971) is used to simulate heat loss to the cylinder walls applying also a turbulence sub-model. During transient operation, the thermal inertia of the cylinder wall is taken into account, using a detailed heat transfer scheme that models the temperature distribution from the gas to the cylinder wall up to the coolant (Rakopoulos and Giakoumis, 2009).

2.2 Dynamics of the slider–crank mechanism: detailed connecting rod modelling

At each instant of time, the displacement of the piston from the Top Dead Centre (TDC) is given by

$$x(\theta) = r(1-\cos\theta) + L_{rod}\left(1 - \sqrt{1 - \lambda^2 \sin^2\theta}\right) \tag{1}$$

where r is the crank radius, $\lambda = r/L_{rod}$ with L_{rod} the connecting rod length (see also Figure 1), and θ is the crank angle.

Figure 1　Schematic diagram of the slider–crank mechanism, illustrating forces and torques for the computation of the total inertia force acting on the crankpin
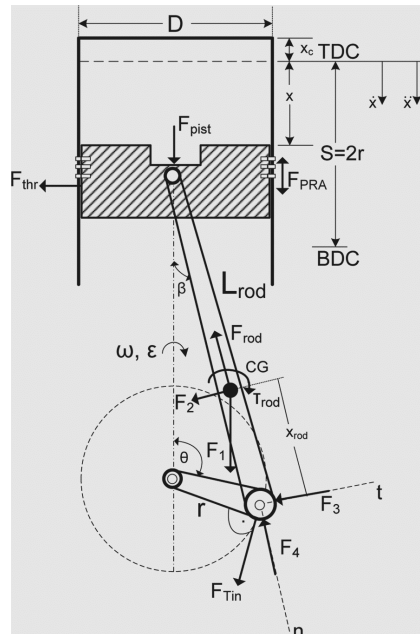
Differentiating the above-mentioned equation with respect to time, we get the instantaneous piston velocity

$$\dot{x}(\theta) = \omega r \sin\theta \left(1 + \frac{\lambda\cos\theta}{\sqrt{1 - \lambda^2\sin^2\theta}} \right) \tag{2}$$

and differentiating once again with respect to time, we get the instantaneous piston acceleration

$$\ddot{x}(\theta) = \omega^2 r \left(\cos\theta + \lambda\frac{\cos 2\theta + \lambda^2\sin^4\theta}{(1 - \lambda^2\sin^2\theta)^{3/2}} + \frac{1}{\omega^2}\varepsilon\frac{\dot{x}(\theta)}{r\omega} \right). \tag{3}$$

The last term on the right-hand side of equation (3) takes into account the influence of the crank's angular acceleration, $\varepsilon = d\omega/dt$ on the piston linear acceleration.

In the literature, the connecting rod is usually modelled as equivalent to two-lumped masses concentrated at its ends, i.e., one reciprocating with the piston assembly and the other rotating with the crank pin (Taylor, 1985). This approach is widely adopted for simplicity reasons. However, it induces errors in the slider–crank mechanism dynamics (of the order of a few percentage points) by miscalculating the actual rod's moment of inertia and the various forces of the kinematic mechanism. For a more accurate computation of engine (inertia) torque, the present research group has developed a detailed model of the connecting rod based on rigid body dynamics (Rakopoulos et al., 2007). Here, we analyse the complex, elliptical movement of the rod's Centre of Gravity (CG) that is produced by its reciprocating and rotating motion providing a 3 by 3 system of algebraic equations that can be solved for the unknown forces F_{thr}, F_3 and F_4 (Figure 1). Force F_{thr} is the inertia component of the thrust force acting by the piston on the side wall of the cylinder. The sum of the projections of forces F_3 and F_4 on an axis perpendicular to the crank radius produces the tangential (inertia) force F_{Tin}, owing to the inertia of the moving parts (piston assembly and connecting rod) acting on the crank, i.e.

$$F_{Tin} = F_3\cos(\theta + \beta) + F_4\sin(\theta + \beta). \tag{4}$$

The latter will be used in the next section for the computation of the engine-indicated torque. However, according to the previous research by the same group (Rakopoulos et al., 2007), inclusion of the connecting rod true motion only marginally affects the obtained results.

2.3 *Crankshaft torsional behaviour model*

The engine under study is an in-line, six-cylinder, turbocharged and after-cooled diesel engine; its basic data are given in Table 1.

In the simplified torsional behaviour approach, a condensed crankshaft model is adopted that is assumed rigid enough between the cylinder cranks and elastic in the power transmission shaft between flywheel and load. The respective engine–load angular momentum equilibrium is formulated as follows, with reference to the upper sub-diagram of Figure 2 (Rakopoulos and Giakoumis, 2009).

$$\tau_{e1}(\theta) - k_L(\theta - \theta_L) - C_L(\dot{\theta} - \dot{\theta}_L) = (G_e + G_{fl} + G_{coupl})\frac{d\omega}{dt}$$

$$k_L(\theta - \theta_L) + C_L(\dot{\theta} - \dot{\theta}_L) - \tau_L(\theta_L) = G_L\frac{d\omega_L}{dt}$$

(5)

where τ_{e1} is the total (from all cylinders) engine brake torque (indicated minus friction), $k_L(\theta - \theta_L)$ is the stiffness torque of the connecting shaft, $C_L(\dot{\theta} - \dot{\theta}_L)$ is the damping torque, $\omega = \dot{\theta}$ is the engine angular velocity and $\omega_L = \dot{\theta}_L$ is the load angular velocity. Moreover, G_e, G_{fl}, G_{coupl} and G_L are the mass moments of inertia of the engine, flywheel, elastic coupling (if present), and load, respectively.

Table 1   Basic data for engine and turbocharger

Engine model and type	In-line, six-cylinder, four-stroke, compression ignition, turbocharged, after-cooled, heavy-duty
Speed range	1000–1500 rpm
Bore/Stroke	140 mm/180 mm
Ignition order	1-5-3-6-2-4
Difference between successive firing cylinders	120 deg. CA
Maximum power	320 HP (236 kW) @ 1500 rpm
Maximum torque	1520 Nm@1250 rpm
Turbocharger	Single-stage, centrifugal compressor, Single-stage, twin entry, axial turbine
Moment of inertia	Engine and Brake: 15.60 kg m^2 Turbocharger: 7.5×10^{-4} kg m^2

For the present analysis, a more detailed engine–load torsional behaviour system is chosen assuming the crankshaft as a flexible, elastic body that may deform during engine operation. Simulation is accomplished using the lumped mass model depicted in the lower sub-diagram of Figure 2. The elastic crankshaft rotary motion is excited by the gas and inertia torque fluctuation. For the in-line, six-cylinder engine under study, the following nine, non-linear differential equations apply

$$G_{aux} \cdot \ddot{\theta}_{aux} + C_{aux} \cdot (\dot{\theta}_{aux} - \dot{\theta}_6) + k_{aux} \cdot (\theta_{aux} - \theta_6) = \tau_{aux}$$

$$G_{cyl} \cdot \ddot{\theta}_6 + C_{aux} \cdot (\dot{\theta}_6 - \dot{\theta}_{aux}) + C_{cyl} \cdot (\dot{\theta}_6 - \dot{\theta}_5) + k_{aux} \cdot (\theta_6 - \theta_{aux}) + k_{cyl} \cdot (\theta_6 - \theta_5) = \tau_{e6}$$

$$G_{cyl} \cdot \ddot{\theta}_5 + C_{cyl} \cdot (\dot{\theta}_5 - \dot{\theta}_4) + C_{cyl} \cdot (\dot{\theta}_5 - \dot{\theta}_6) + k_{cyl} \cdot (\theta_5 - \theta_4) + k_{cyl} \cdot (\theta_5 - \theta_6) = \tau_{e5}$$

$$G_{cyl} \cdot \ddot{\theta}_4 + C_{cyl} \cdot (\dot{\theta}_4 - \dot{\theta}_5) + C_{cyl} \cdot (\dot{\theta}_4 - \dot{\theta}_3) + k_{cyl} \cdot (\theta_4 - \theta_5) + k_{cyl} \cdot (\theta_4 - \theta_3) = \tau_{e4}$$

$$G_{cyl} \cdot \ddot{\theta}_3 + C_{cyl} \cdot (\dot{\theta}_3 - \dot{\theta}_4) + C_{cyl} \cdot (\dot{\theta}_3 - \dot{\theta}_2) + k_{cyl} \cdot (\theta_3 - \theta_4) + k_{cyl} \cdot (\theta_3 - \theta_2) = \tau_{e3} \qquad (6)$$

$$G_{cyl} \cdot \ddot{\theta}_2 + C_{cyl} \cdot (\dot{\theta}_2 - \dot{\theta}_3) + C_{cyl} \cdot (\dot{\theta}_2 - \dot{\theta}_1) + k_{cyl} \cdot (\theta_2 - \theta_3) + k_{cyl} \cdot (\theta_2 - \theta_1) = \tau_{e2}$$

$$G_{cyl} \cdot \ddot{\theta}_1 + C_{cyl} \cdot (\dot{\theta}_1 - \dot{\theta}_2) + C_{fl} \cdot (\dot{\theta}_1 - \dot{\theta}_{fl}) + k_{cyl} \cdot (\theta_1 - \theta_2) + k_{fl} \cdot (\theta_1 - \theta_{fl}) = \tau_{e1}$$

$$(G_{fl} + G_{coupl}) \cdot \ddot{\theta}_{fl} + C_{fl} \cdot (\dot{\theta}_{fl} - \dot{\theta}_1) + C_l \cdot (\dot{\theta}_{fl} - \dot{\theta}_L) + k_{fl} \cdot (\theta_{fl} - \theta_1) + k_L \cdot (\theta_{fl} - \theta_L) = \tau_{fl}$$

$$G_L \cdot \ddot{\theta}_L + C_L \cdot (\dot{\theta}_L - \dot{\theta}_{fl}) + k_L \cdot (\theta_L - \theta_{fl}) = \tau_L$$

Cylinder number and disposition play a vital role in structuring equation (6), as different engine architectures lead to different equation formulations, affecting strongly all the derived results. Equation (6) is transformed from a time basis on a °CA basis using the well-known relation $d\theta = 6\,N\,dt$, with N the instantaneous engine speed (calculated at each integration step).

In the above-mentioned equations, G_{aux} is the auxiliaries mass moment of inertia and G_{cyl} is the individual cylinder moment of inertia comprising reciprocating ('rec') and rotating ('rot') masses contribution; G_{cyl} is given by the following equation

$$G_{cyl} = G_{rec} + G_{rot} \approx \frac{1}{2}m_{rec}r^2 + m_{rot}r^2. \tag{7}$$

A more detailed computation of cylinder moment of inertia is provided in Rakopoulos and Giakoumis (2009).

Figure 2 Schematic arrangement of the engine–load dynamic system for crankshaft torsional behaviour modelling
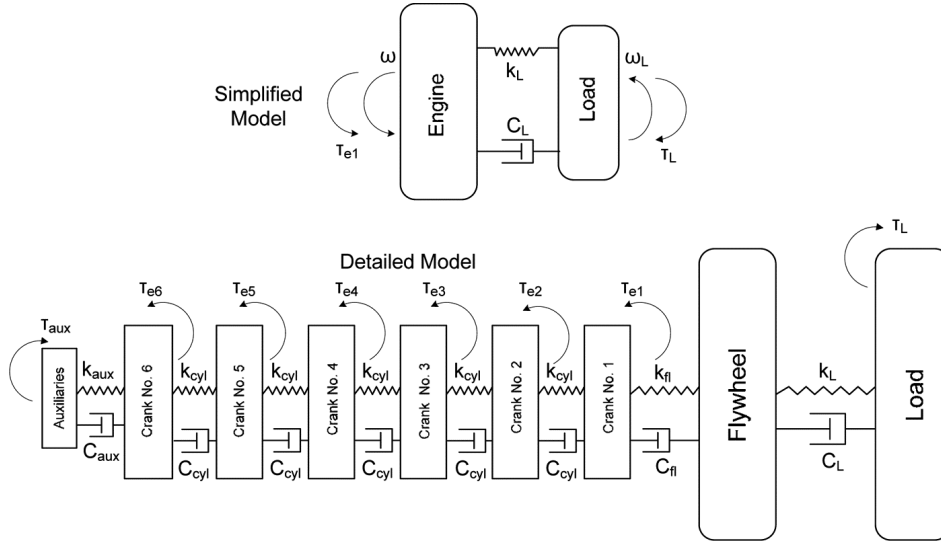
Further in Figure 2 and equation (6), τ_{ei} ($i = 1,\ldots, 6$) denotes the total engine brake torque up to cylinder crank 'i' considered. The calculation of an individual cylinder torque term is mostly dependent on accurate combustion modelling and is given explicitly by the following equation (Taylor, 1985)

$$\tau_e(\theta) = \overbrace{\left[\tau_g(\theta) + \tau_{in}(\theta)\right]}^{\text{indicated torque}} - \tau_{fr}(\theta) = \left[\left(p_g(\theta) \cdot A_{pist} \cdot \frac{\dot{x}(\theta)}{r\omega}\right) + F_{Tin}(\theta)\right] \cdot r - \tau_{fr}(\theta). \tag{8}$$

In the above-mentioned relation, $p_g(\theta)$ is the instantaneous cylinder gas pressure computed from the single-zone thermodynamic analysis of the cylinder processes discussed in Section 2.1. $\tau_{fr}(\theta)$ is the instantaneous friction torque (discussed later) and F_{Tin} is the torsional inertia force calculated from equation (4). All torque terms in equation (8) are illustrated in Figure 5 later in the text.

For the various intermediate positions (between successive cranks) '*i*' in the crankshaft, the corresponding engine total brake torque τ_{ei} from all cylinders up to that point, needed in equation (6), is given by equation (9) with reference to Figures 2 and 3. These relations are formulated according to the specific engine firing order (1-5-3-6-2-4); the latter is typical of turbocharged, in-line, six-cylinder engines for best balancing.

$$\tau_{e6} = \tau_e(\theta)$$
$$\tau_{e5} = \tau_{e6} + \tau_e(\theta + 4 \cdot \theta_{\text{ign}})$$
$$\tau_{e4} = \tau_{e5} + \tau_e(\theta + 2 \cdot \theta_{\text{ign}})$$
$$\tau_{e3} = \tau_{e4} + \tau_e(\theta + 5 \cdot \theta_{\text{ign}}) \qquad (9)$$
$$\tau_{e2} = \tau_{e3} + \tau_e(\theta + 1 \cdot \theta_{\text{ign}})$$
$$\tau_{e1} = \tau_{e2} + \tau_e(\theta + 3 \cdot \theta_{\text{ign}}).$$

Figure 3 Diagram showing the (in-line six-cylinder engine) crank star for 1-5-3-6-2-4 ignition order and equal firing intervals
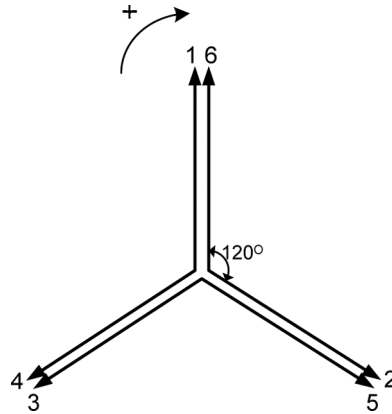
For the calculation of engine friction, the model proposed by Taraza et al. (2000) is applied. It describes the non-steady profile of friction torque during each cycle, based on fundamental friction analysis. In the adopted model, the total amount of friction is divided into four parts, i.e., PRA, loaded bearings, valve train and auxiliaries. The important outcome is that this friction torque varies during the engine cycle, especially around 'hot' TDC, unlike the usually applied 'mean' fmep (friction mean effective pressure) equations, where friction torque remains constant throughout each cycle. PRA, loaded bearings and valve train friction contribution are accounted for in term $\tau_{fr}(\theta)$ in equation (8). On the other hand, the auxiliaries (water-, oil-, fuel pump, etc.) term, $\tau_{\text{aux}}(\theta) \propto \omega$, is calculated separately and used in the first of equation (6).

Finally, τ_L is the load torque, which can be approximated by the following relation

$$\tau_L(\theta_L) = \alpha_1 + \alpha_2 \omega_L^s. \qquad (10)$$

For a linear load-type (i.e., electric brake, generator) $s = 1$, while for a quadratic load-type (i.e., hydraulic brake, fixed pitch propeller, vehicle aerodynamic resistance) $s = 2$, with 'α' the speed-independent load term (e.g., road slope).

In equation (6), the terms $k_{ij}(\theta_i - \theta_j)$, where i and j are each cylinder crank ('1'…'6'), flywheel ('*fl*'), auxiliary gears ('aux') or load ('*L*') represent the respective torsional stiffness torque of the shaft between each examined 'pair' $i - j$, while the damping torque is identified by the $C_{ij}(\dot{\theta}_i - \dot{\theta}_j)$ terms. Further, k_{ij} is the individual stiffness and C_{ij} is the individual damping coefficient of each shaft part examined (e.g., between cylinder cranks 5 and 4, or between flywheel and load, etc.)

Differential equation (6) is solved at each ºCA, using the instantaneous torque terms from each one of the six cylinders of the present engine. Particularly, as regards the gas torque during transients, the individual cylinder gas pressures are derived from the thermodynamic model, with application of the 'true multi-cylinder' approach described in the next section. Solution of equation (6) provides the individual rotational speeds and the respective angles θ_i, hence the torsional deformation $\Delta\theta = \theta_i - \theta_j$.

2.4 Transient operation

Various sophisticated sub-models, which analyse important engine features during transient operation, have been incorporated in the main simulation code; details can be found in Rakopoulos et al. (2004), Rakopoulos and Giakoumis (2006a, 2006b). A brief description is provided here.

Multi-cylinder engine modelling. At steady-state operation, the performance of each cylinder is essentially the same, owing to the constant position of the governor clutch resulting in the same amount of fuel being injected per cycle, and the constant turbocharger compressor operating point. Under transient operation, however, each cylinder experiences *different* fuelling and air mass flow-rate during the same engine cycle. This happens due to the combined effect of:

- the continuous movement of the fuel pump rack that is initiated by a load or speed change

- the continuous movement of the turbocharger compressor operating point.

As regards speed changes, only the first cycles are practically affected. However, when load changes are investigated, significant variations can be experienced throughout the whole transient cycle. The usual approach, here, is the solution of the governing equations for one cylinder and the subsequent use of suitable phasing images of this cylinder's behaviour. This approach is widely popular for limiting the computational time (Rakopoulos and Giakoumis, 2006b). Unlike this, the present research group has developed a true 'multi-cylinder' engine model. Here, all the governing differential and algebraic equations are solved individually for every one cylinder of the six-cylinder engine under study, according to the current values of the fuel pump rack position and turbocharger compressor flow. This results in (significant) differentiations in both fuelling and air mass flow-rates for each cylinder during the *same* cycle of a transient event, affecting, among other things, the crankshaft torsional deformation results.

Fuel pump operation. Instead of using steady-state fuel pump curves during transients, a fuel injection model, experimentally validated at steady-state conditions, is employed. Thus, simulation of the fuel pump-injector lift mechanism is accomplished, taking into account the delivery valve and injector needle motion. The unsteady gas flow equations are solved using the method of characteristics, providing the dynamic injection timing as

well as the duration and the rate of injection for each cylinder at each transient cycle. The obvious advantage here is that the *transient* operation of the fuel pump is also taken into account. This is mainly accomplished through the fuel pump residual pressure value, which is built up together with the other variables during the transient event.

3   Results and discussion

The experimental investigation was conducted on a heavy-duty, six-cylinder, turbocharged diesel engine, the basic data of which are provided in Table 1. Details about the experimental procedure and the matching between simulated and experimental results concerning engine performance can be found in Rakopoulos et al. (2004). After gaining confidence in the model's predictive capabilities, the simulation analysis of the crankshaft torsional deformation effects was carried out.

Figure 4 illustrates the development of the torsional deformation between engine flywheel and load, using the 2-term torsional behaviour model of equation (5), during typical, steady-state, diesel engine operation. A 'single-cylinder version' of the current engine is initially chosen for the analysis, in order for the results to be directly comparable with the in-cycle pressure and torque build-up. The data presented in Figure 4 are in accordance with the findings of previous research at steady-state conditions (Chen and Chen, 1993; Du, 1999), as regards both in-cycle profile and absolute values. Figure 4 should be studied in conjunction with Figure 5 that depicts the development of all torque contributors during the same engine cycle (according to equation (8)). The instantaneous total engine torque in Figure 5 (not shown) closely follows its gas torque counterpart profile.

Figure 4   Development of power transmission shaft torsional deformation and engine speed during steady-state, single-cylinder engine operation
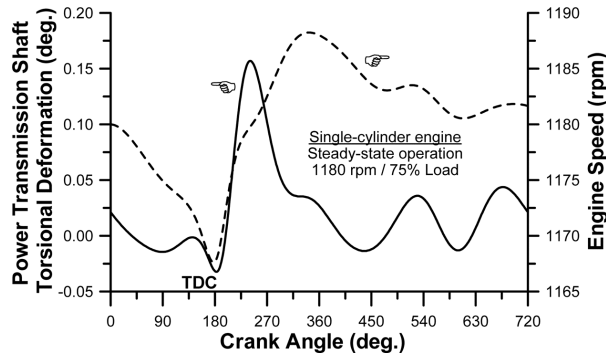
During compression (0–180°CA), there is a deficit of gas torque that leads to engine speed decrease and the 'negative' crankshaft deformation shown in Figure 4; torque, speed and deformation all peak around 'hot' TDC. After the start of combustion, there is a surplus of torque, as now the engine enters the power production phase of operation. Consequently, 'positive' deformation is established, while the instantaneous engine speed increases; this lasts for the whole expansion stroke. The considerably higher amount of engine torque produced during expansion leads to the greater local peak in crankshaft

deformation, i.e., 0.16 deg occurring at about 55 CA after 'hot' TDC, compared with the local minimum of −0.03 deg at 180 CA.

The main mechanism behind the crankshaft torsional deformation profile, over an engine cycle, is clearly the gas torque because of its direct impact on the total engine torque. Instantaneous values of gas torque are, among other things, strongly affected by the injection rate and profile, which, in turn, influence the smoothness or roughness of the engine operation. Closer examination of Figure 4 reveals that inertia torque influence is also present, mainly during the open part of the cycle where the cylinder pressure is low, as well as during the second half of compression. For the present engine, the inertia contribution is rather small due to the low engine speed (recall that inertia forces vary as the square of the engine speed).

Another interesting finding is that stiffness and damping instantaneous torques may reach high values during an engine cycle. The profile of stiffness torque follows the torsional deformation as described earlier. The profile of damping torque (damping coefficient value assumed based on bibliographic data for similar engine–load configurations) is indicative of the instantaneous difference between engine and load speeds. Owing to the 'internal inertia' of these 'processes', the respective torque peaks observed in the upper sub-diagram of Figure 5 may be delayed compared with the initiating gas torque or cylinder pressure. However, despite their relatively high instantaneous values, both stiffness and damping torques' mean (over the engine cycle) values are negligible compared with the gas or load torque. As a result, the usually applied assumption is justified, i.e., neglecting these torques for the calculation of *mean* engine speed. For lower engine loads, or for higher stiffness, overall lower deformation values are experienced. Likewise, smaller deformations are expected for naturally aspirated diesel or for spark ignition engines, where the cylinder pressures are much lower. In the latter cases, a greater influence of inertia torque is also observed, particularly so for the small automotive engines operating at high rotational speeds.

Figure 5 Various torque contributors' build-up during steady-state, single-cylinder engine operation (all three ordinates correspond to torque values)
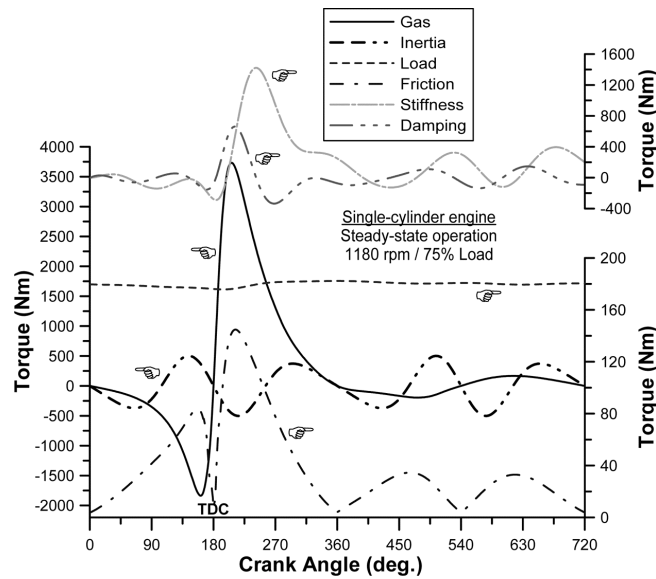
The main findings of the 'single cylinder' configuration can be extended to the (real) multi-cylinder engine operation, which is depicted in Figure 6 for two engine loads,[2] namely 50 and 90% of the full engine load at 1180 rpm. The effect of the number of cylinders is the dominant factor in the multi-cylinder analysis of Figure 6. In fact, the torsional deformation frequency for the four-stroke, six-cylinder engine is, as expected, $720°/6 = 120°$. Contrary to the single-cylinder results, there is always an adequate surplus of gas torque that prevents the crankshaft torsional deformation from reaching negative values.

Figure 6   Development of torsional deformation between engine flywheel and load during steady-state, multi-cylinder engine operation at 1180 rpm engine speed
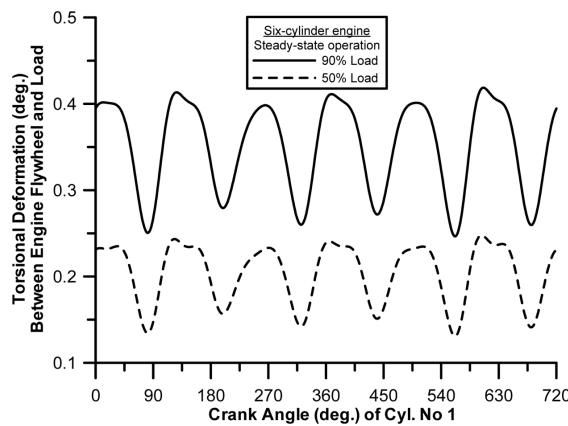
Figure 7 expands on the previous results by focusing on the instantaneous torsional deformations between the various cylinder cranks. The important findings from this figure are:

Figure 7   Development of torsional deformation between individual cylinder cranks during steady-state engine operation
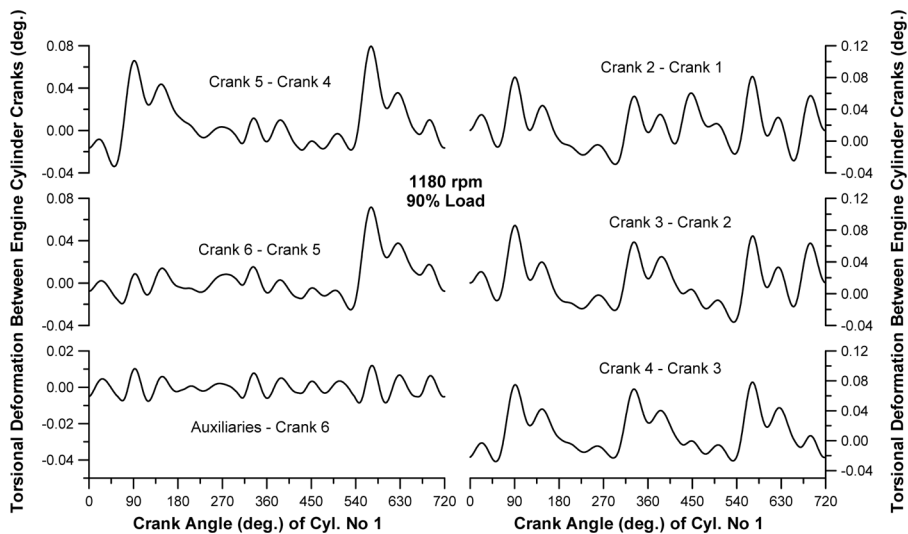
1 The magnitude of the intra-crank deformations is always of much lower importance owing to the shorter length of the shaft between two consecutive cranks, which increases considerably the corresponding stiffness coefficient k, as is also dictated by the following equation

$$k = \frac{\Theta J_p}{\ell} \tag{11}$$

where Θ is the shear modulus (modulus of rigidity), $J_p = \pi d^4 / 32$ is the shaft polar moment of inertia, and d and ℓ are the shaft diameter and length, respectively.

2 The development of the intra-crank deformation profile incorporates the corresponding engine torque fluctuation up to the point considered, following equation (9); the latter effect is further demonstrated in Figure 8 for comparison purposes. As a result, the closer a crank to the flywheel the greater the number of engine cylinders that contribute with their individual torques to its deformation, hence the higher its torsional deformation irregularity and stress; stress σ is defined by

$$\sigma = \frac{\Theta}{2} \frac{d}{\ell} \Delta\theta.$$

Figure 8 Development of cumulative indicated (gas and inertia) engine torque at the various crankshaft positions during steady-state engine operation
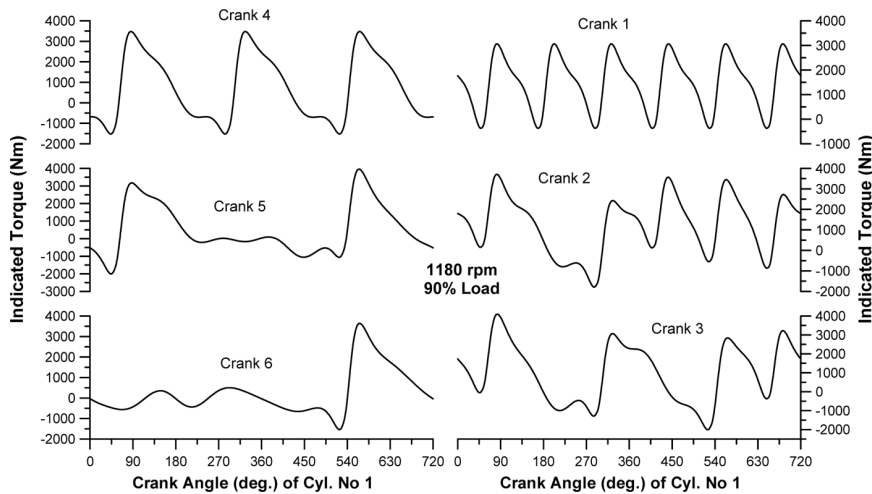
Two interesting malfunctioning cases are examined in Figure 9. In the first case, cylinder No. 4 operates under an 'open valve' condition, which means that both the inlet and the exhaust valves are continuously open during the whole engine cycle. In the second case, there is no fuel injection and combustion in cylinder No. 4, which is motored by the other five cylinders. For both cases, a significant dip in the torsional deformation is observed, owing to the absence of the dominant gas torque contribution from the specific cylinder. The situation is much more pronounced during the 'open valves' condition owing to the fact that, here, there is neither compression nor expansion; the respective $p_g(\theta)$ term in equation (8) for cylinder No. 4 equals, in this case, the manifold pressure.

The upper sub-diagram of Figure 9 focuses on a typical intra-cylinder (between cranks 3 and 4) deformation for the two examined malfunctioning operating conditions.

Figure 9   Development of torsional deformation for two special operating cases
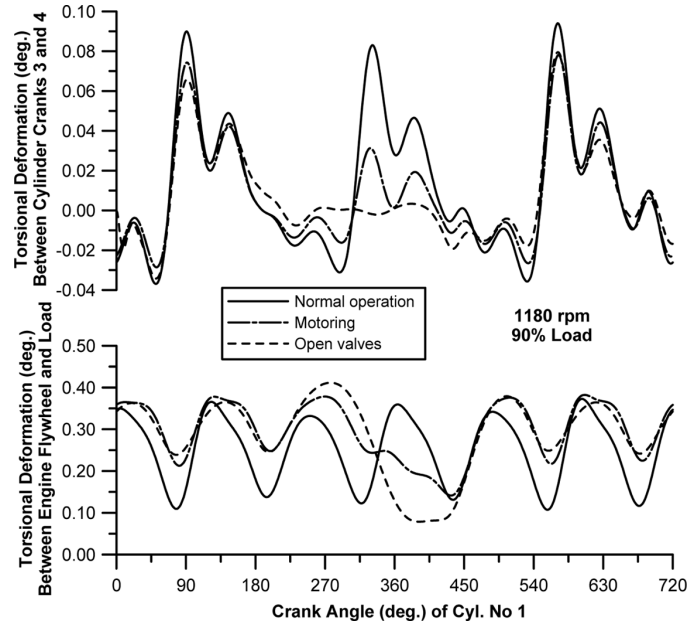
The investigation of the results during transient operation was the next task. Owing to the narrow speed range of the engine in hand, mainly load increases under constant governor setting were investigated, which, nonetheless, play a significant role in the European or American Transient Cycles of heavy-duty vehicles. In addition, since engine load affects torsional deformation in a much more prominent way compared with rotational speed, it seems quite reasonable to focus on load increases.

The most notable off-design feature of diesel engine transient operation that significantly differentiates the torque pattern from the respective steady-state conditions is the turbocharger lag. This is caused because, although the fuel pump responds rapidly to the increased fuelling demand after a load or speed increase, the turbocharger compressor air-supply cannot match this higher fuel-flow instantly, but only after a number of engine cycles owing to the inertia of the whole system (since there is no mechanical connection between engine crankshaft and turbocharger); the above-mentioned phenomenon is enhanced by the unfavourable turbocharger compressor characteristics at low loads and speeds. As a result of this slow reaction, the relative air–fuel ratio during the early cycles of a transient event assumes very low values (even lower than stoichiometric), thus deteriorating combustion and leading to slow engine (torque and speed) response, long recovery period, and overshoot in particulate, gaseous and noise emissions (Rakopoulos and Giakoumis, 2009).

Figure 10 depicts the development of the maximum and the mean, over each engine cycle, deformation for the flywheel–load and for the location between cylinder cranks 2 and 3 for a typical load increase transient event of 10–80% commencing from an engine speed of 1180 rpm. Initially, the deformation is negligible because of the low

engine load. As the governor responds to the drop in engine speed caused by the abrupt load increase, the fuelling increases too (right-hand side sub-diagram of Figure 10) leading to higher gas pressures $p_g(\theta)$ and torques throughout the cycle following equation (8). This results in greater maximum and mean, over the engine cycle, deformations (cf. Figure 6). It is important to note that the instantaneous maximum deformations are considerably higher (up to 30% for the cases examined in this work) than the respective mean values in the same cycle. Consistent with the steady-state results presented in Figure 7, the crankshaft deformation between cylinder cranks Nos. 2 and 3 is always of much lower magnitude compared with the flywheel–load one.

Figure 10 Development of maximum and mean, over an engine cycle, torsional deformation during a 10–80% load increase transient event
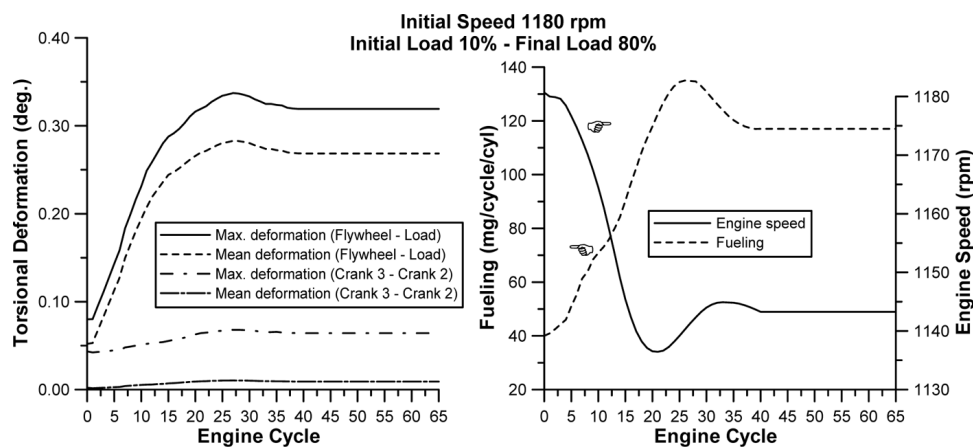
It should be pointed out here that the evolution of transient maximum or mean, over the engine cycle, deformation (and stress) develop in a different way and assume different values compared with the corresponding steady-state engine operation points (i.e., at the same engine speed and fuel pump rack position). The difference is, mainly, attributed to:

- the different air–fuel equivalence ratios experienced during transients owing to the turbocharger lag, which significantly affects the air–mass flow rate, particularly during the early cycles of the transient event

- the transient operation of the fuel pump that differentiates from the steady-state fuel pump curves.

To evaluate the importance of the 9-part differential equation scheme (equation (6)) compared with the simplified 2-part term (equation (5)), Figure 11 is provided. Unsurprisingly, the analytical deformation procedure produces differentiated instantaneous and mean values, owing to the much more detailed formulation of the crankshaft torsional behaviour. This fact justifies the decision to study this dynamic phenomenon on a detailed °CA basis, to be able to ultimately estimate the 'true' maximum stress that is experienced by each engine part during a load increase transient event.

Figure 11 Comparison in the torsional deformation prediction between the simplified and analytical torsional behaviour models depicted in Figure 2
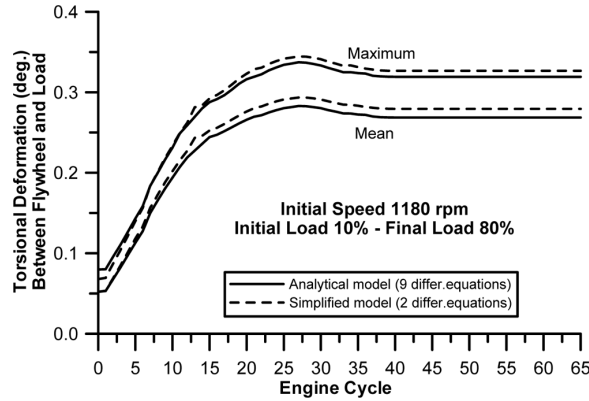
The transient results are expanded in Figure 12, by showing the 'wave' of (crank)shaft deformation build-up for several cycles of the same transient event. Closer examination of the curves in Figure 12 reveals that the increase in loading/fuelling ultimately leads to greater in-cycle fluctuations of the deformation too. The rather slow development of the transient event owing to the high engine–load mass moment of inertia is reflected into slow deformation build-up during the early cycles 1–5.

Figure 12 Development of torsional deformation between flywheel and load and between cylinder cranks 3 and 4 during various cycles of the 10–80% load increase transient event
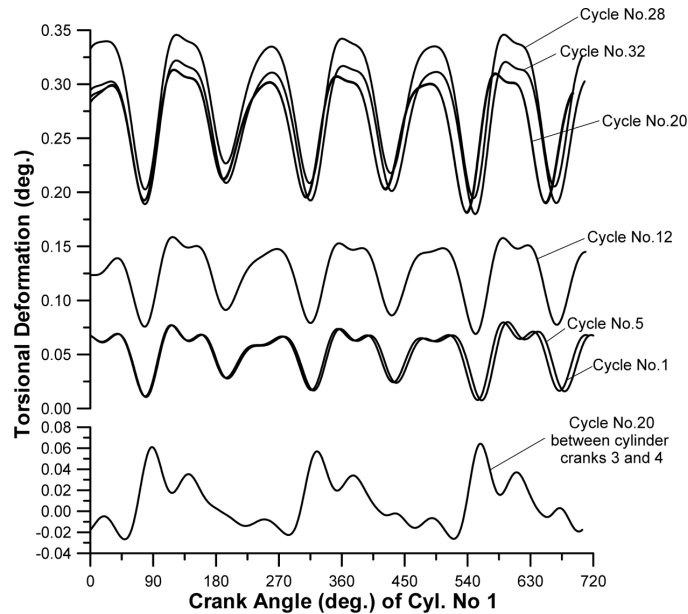
From the previous analysis, it has been made evident that, in principle, the main parameters affecting the profile and values of (crank)shaft torsional deformations are the

applied engine load and the shaft stiffness. The effect of loading during transients is further demonstrated in the upper sub-diagram of Figure 13. The higher the applied load, the higher the torque deficit during the early cycles of the transient event. This, in turn, leads to a 'harder' turbocharger lag period, lower air–fuel ratio, higher crankshaft deceleration and lower engine speed, thus initiating larger governor displacement, greater fuel pump rack position, and higher values of engine torque and peak cylinder pressure. Consequently, after the start of combustion, the surplus of net torque is much higher now resulting in greater peaks of crankshaft deformation as was also anticipated from the steady-state results shown in Figure 6. The above-mentioned phenomenon is enhanced the more rigid the resistance connected to the engine (lower values of exponent '*s*' in equation (10)).

Figure 13 Effect of various parameters on (crank)shaft torsional deformation during transient operation after a load increase
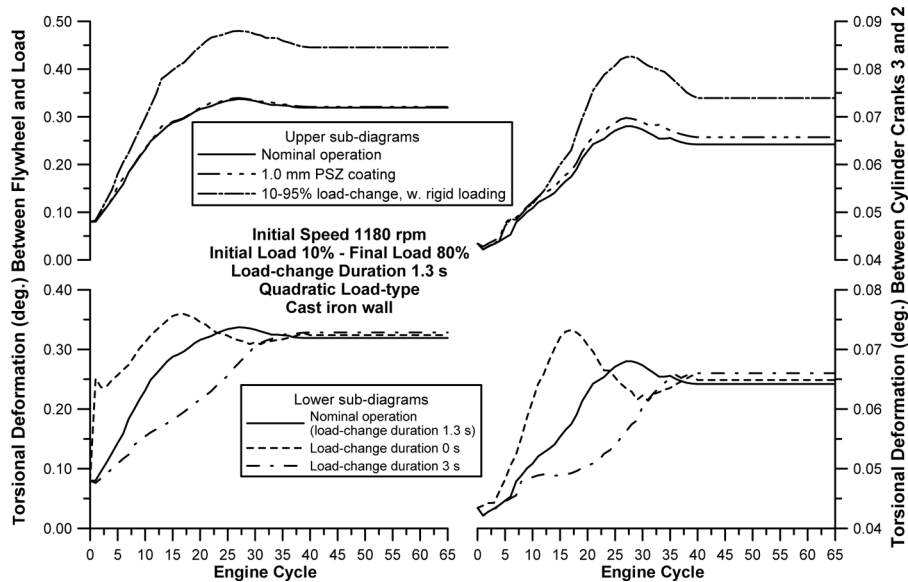
Two other interesting parameters are investigated in Figure 13, namely the load-change schedule of the transient event Δt_{load} and the cylinder wall insulation.

As discussed earlier (remarks concerning Figure 10), the torsional deformation profile follows closely its fuelling counterpart (not shown), and appears to be significantly affected by the load-time schedule (lower sub-diagram of Figure 13). Consistent with engineering intuition, the final equilibrium conditions are practically the same for all the cases examined. The most demanding case is the one with instant load application ($\Delta t_{load} = 0$). Here, the load torque increases instantly reaching its final value during the first transient cycle, while its engine counterpart responds with a delay, following the governor response to the speed drop. Consequently, there is a considerable torque deficit during the first cycles of the transient event that leads to earlier, and higher deformations compared with the nominal case ($\Delta t_{load} = 1.3$ s). A pulsating form of engine recovery may also be observed in this case, which is unacceptable, but this depends on the specific governor characteristics. On the other hand, a long load-change duration ($\Delta t_{load} = 3.0$ s)

causes smoother development of the crankshaft deformation, as the whole transient event develops at a much slower, hence 'safer' rate.

The very interesting case of insulated cylinder walls, resembling a Low Heat Rejection (LHR) engine, is also investigated in the upper sub-diagram of Figure 13 for the case where the cylinder wall is coated with 1 mm of Plasma Spray Zirconia (PSZ). The objective of an LHR engine is to minimise heat loss to the cylinder walls, eliminating in that way the need for a cooling system. This is achieved at the expense of increased levels of gas temperatures inside the cylinder, resulting from the insulation applied to the cylinder walls, piston crown, cylinder head and valves. On the other hand, gas pressures are influenced too but at a much more moderate level. The insulation effect on engine and turbocharger transient response has been reported to be rather limited except for the NO emissions (Borman and Nishiwaki, 1987; Rakopoulos et al., 2008). Since torsional deformation is mainly affected by gas pressure rather than temperature, the PSZ-insulated cylinder wall engine in Figure 13 exhibits overall only slightly higher torsional deformations compared with the un-insulated operation.

4   Summary and conclusions

An experimentally validated simulation code has been used to study the development of crankshaft torsional deformations during steady-state and transient operation of a turbocharged diesel engine.

When formulating the crankshaft angular momentum equilibrium, care was taken to apply *instantaneous* values for all torque terms, including engine friction (using a detailed model), stiffness and damping, whereas the gas torque contribution was computed separately for each cylinder using a 'real multi-cylinder' engine model.

Application of the detailed 9-part differential equation crankshaft torsional behaviour model helped in quantifying crankshaft torsional deformation values during steady-state and transient operation. Improved understanding of contributing and controlling factors is believed to have been achieved. From the analysis of the present (in-line, six-cylinder) engine–load configuration, the following results were reached:

- Engine torque was identified as the main contributor in crankshaft deformation profile and peak values. Inertia torque influences the crankshaft deformation mainly during the open part of the cycle (of a single-cylinder engine), but it was overall limited for the present engine owing to its, relatively, low speed.

- Stiffness and damping torques can reach significant instantaneous values during a cycle. However, their mean, over the engine cycle, values are negligible compared with the engine and load terms.

- Local deformation between individual cylinder cranks is always of much lower importance, because of the considerably higher stiffness coefficients involved. The closer the examined crankshaft part is to the flywheel, the higher its torsional deformation irregularity and stress.

- Mean and maximum, over an engine cycle, deformation response can assume significant values during transient operation, depending on the load increase schedule. The instantaneous maximum deformation can be at least 30% higher (for the case examined) compared with the respective mean value in the same

transient cycle. The same holds true for the respective crankshaft stress, which, however, never reached the plastic deformation limit for the engine in hand.

- The transient deformations develop in a different way compared with the corresponding steady-state operating points, owing to the differentiated fuelling and air–mass flow rates experienced during transients, following turbocharger lag.

- Higher load changes as well as more rigid construction of the crankshaft were identified as key parameters of the torsional deformation profile during transients. The load-change schedule was found quite influencing, particularly so the more instant the load application. On the other hand, insulating the cylinder walls only marginally influences the crankshaft deformation and stress.

References

Annand, W.J.D. and Ma, T.H. (1970–1971) 'Instantaneous heat transfer rates to the cylinder head surface of a small compression ignition engine', *Proceedings of the Institution of Mechanical Engineers*, Vol. 185, pp.976–987.

Benson, R.S. and Whitehouse, N.D. (1979) *Internal Combustion Engines*, Pergamon Press, Oxford, UK.

Black, J., Eastwood, P.G., Tufail, K., Winstanley, T., Hardalupas, Y. and Taylor, A.M.K.P. (2007) *Diesel Engine Transient Control and Emissions Response during a European Extra-Urban Drive Cycle (EUDC)*, SAE Paper No. 2007-01-1938.

Borman, G. and Nishiwaki, K. (1987) 'Internal-combustion engine heat transfer', *Progress in Energy and Combustion Science*, Vol. 13, pp.1–46.

Chen, S.K. and Chen, S. (1993) *Engine Diagnostics by Dynamic Shaft Measurement: A Progress Report*, SAE Paper No. 932412.

Du, H.Y.I. (1999) *Simulation of Flexible Rotating Crankshaft with Flexible Engine Block and Hydrodynamic Bearings for a V6 Engine*, SAE Paper No. 1999-01-1752.

Haddad, S.D. (1995) 'Theoretical treatment of piston motion in I.C. piston engine for the prediction of piston slap excitation', *Mechanism and Machine Theory*, Vol. 30, pp.253–269.

Haug, K. (1952) *Die Drehschwingungen in Kolbenmaschinen*, Springer-Verlag, Berlin/Goettingen/Heidelberg.

Heywood, J.B. (1988) *Internal Combustion Engine Fundamentals*, McGraw-Hill, New York, NY.

Ker Wilson, K. (1959–1969) *Practical Solution of Torsional Vibration Problems*, 3rd ed., Chapman and Hall, London, UK.

Murin, J. (2005) 'Some properties of a diesel drive line with hydrodynamic torque converters of the latest generation', *Mechanism and Machine Theory*, Vol. 40, pp.99–117.

Rahnejat, H. (2000) 'Multi-body dynamics: historical evolution and application', *Proceedings of the Institution of Mechanical Engineers, Part C, Journal of Mechanical Engineering Science*, Vol. 214, pp.149–173.

Rakopoulos, C.D. and Giakoumis, E.G. (2006a) 'Review of thermodynamic diesel engine simulations under transient operating conditions', SAE Paper No. 2006-01-0884, Also, *SAE Transactions, Journal of Engines*, Vol. 115, pp.467–504.

Rakopoulos, C.D. and Giakoumis, E.G. (2006b) 'Sensitivity analysis of transient diesel engine simulation', *Proceedings of the Institution of Mechanical Engineers, Part D, Journal of Automobile Engineering*, Vol. 220, pp.87–101.

Rakopoulos, C.D. and Giakoumis, E.G. (2009) *Diesel Engine Transient Operation*, Springer, London, UK.

Rakopoulos, C.D., Giakoumis, E.G. and Dimaratos, A.M. (2007) *Evaluation of Various Dynamic Issues During Transient Operation of Turbocharged Diesel Engine with Special Reference to Friction Development*, SAE Paper No. 2007-01-0136.

Rakopoulos, C.D., Giakoumis, E.G. and Rakopoulos, D.C. (2008) 'Study of the short-term cylinder wall temperature oscillations during transient operation of a turbocharged diesel engine with various insulation schemes', *International Journal of Engine Research*, Vol. 9, pp.177–193.

Rakopoulos, C.D., Giakoumis, E.G., Hountalas, D.T. and Rakopoulos, D.C. (2004) *The Effect of Various Dynamic, Thermodynamic and Design Parameters on the Performance of a Turbocharged Diesel Engine Operating Under Transient Load Conditions*, SAE Paper No. 2004-01-0926.

Rizzoni, G. and Wang, Y.Y. (1985) 'Estimation of engine torque using nonlinear observers in the crank angle domain', *ASME Winter Annual Meeting*, San Francisco, CA, DSC-Vol.56/DE-86, pp.189–193.

Taraza, D., Henein, N. and Bryzik, W. (2000) *Friction Losses in Multi-Cylinder Diesel Engines*, SAE Paper No. 2000-01-0921.

Taraza, D., Henein, N.A. and Bryzik, W. (1998) *Determination of the Gas-Pressure Torque of a Multicylinder Engine from Measurements of the Crankshaft's Speed Variation*, SAE Paper No. 980164.

Taylor, C.F. (1985) *The Internal Combustion Engine in Theory and Practice*, Vol. 2, MIT Press, Cambridge, MA.

Watson, N. (1981) *Transient Performance Simulation and Analysis of Turbocharged Diesel Engines*, SAE Paper No. 810338.

Watson, N. and Janota, M.S. (1982) *Turbocharging the Internal Combustion Engine*, McMillan, London, UK.

Whitehouse, N.D. and Way, R.G.B. (1969–1970) 'Rate of heat release in diesel engines and its correlation with fuel injection data', *Proceedings of the Institution of Mechanical Engineers, Part 3J*, Vol. 184, pp.17–27.

Zweiri, Y.H., Whidborne, J.F. and Seneviratne, L.D. (1999) 'Numerical inversion of the dynamic model of a single-cylinder diesel engine', *ASME-ICE Spring Technical Proceedings*, Columbus, OH, Vol. 3, pp.139–149.

Notes

[1]A torsional vibration analysis carried out on the engine revealed that, for the rated speed of 1500 rpm, the engine operates close to resonance with the 3rd harmonic order of the first natural mode. Hence, an elastic coupling is applied.

[2]Since the mass moments of inertia of the 'single' cylinder and the six-cylinder engines are not proportional, no conclusion is meant to be drawn concerning the instantaneous maxima or minima of the angular deformations observed in Figures 4 and 6.

Nomenclature

A	Surface area (m^2)
C	Torsional damping coefficient (Nms/rad)
D	Piston diameter (m)
d	Shaft diameter (m)
F	Force (N)
G	Mass moment of inertia (kg m^2)

k	Torsional stiffness coefficient (Nm/rad)
L_{rod}	Connecting rod length (m)
ℓ	Shaft length (m)
m	Mass (kg)
N	Engine speed (rpm)
p	Pressure (bar)
r	Crank radius (m)
S	Piston stroke (m)
t	Time (s)
x	Piston displacement (m)

Greek symbols

β	Connecting rod angle (deg)
$\Delta\theta$	Crankshaft torsional deformation (deg or rad)
θ	Crank angle (deg)
θ_{ign}	Difference between successive firing cylinders (deg)
σ	Torsional (shear) stress (N/m^2)
τ	Torque (Nm)
ω	Angular velocity (rad/s)

Subscripts

b	Brake
e	Engine (indicated)
eq	Equivalent
fl	Flywheel
fr	Friction
g	Gas
in	Inertia
L	Load
rod	Connecting rod
T	Tangential
thr	Thrust

Superscripts

s	Load exponent

Abbreviations

^{o}CA	Degrees crank angle
BDC	Bottom Dead Centre
CG	Centre of Gravity
rpm	Revolutions per minute
PRA	Piston Rings Assembly
PSZ	Plasma Spray Zirconia
SMD	Sauter Mean Diameter (μm)
TDC	Top Dead Centre